Ultrasonics 52 (2012) 521–529

Contents lists available at SciVerse ScienceDirect

Ultrasonics

journal homepage: www.elsevier.com/locate/ultras

Ultrasonic-assisted manufacturing processes: Variational model and numerical simulations

Amir Siddiq, Tamer El Sayed *

Computational Solid Mechanics Laboratory (CSML), Division of Physicial Science and Engineering, King Abdullah University of Science and Technology (KAUST), Thuwal, Saudi Arabia

ARTICLE INFO

Article history:
Received 23 February 2011
Received in revised form 25 September 2011
Accepted 4 November 2011
Available online 17 November 2011

Keywords:
Porous metal plasticity
Ultrasonic softening
Constitutive model
Finite element analysis
Wire drawing

ABSTRACT

We present a computational study of ultrasonic assisted manufacturing processes including sheet metal forming, upsetting, and wire drawing. A fully variational porous plasticity model is modified to include ultrasonic softening effects and then utilized to account for instantaneous softening when ultrasonic energy is applied during deformation. Material model parameters are identified via inverse modeling, i.e. by using experimental data. The versatility and predictive ability of the model are demonstrated and the effect of ultrasonic intensity on the manufacturing process at hand is investigated and compared qualitatively with experimental results reported in the literature.

1. Introduction

The effect of ultrasonic energy on the deformation behavior of metals and alloys has been under investigation for many decades [3–5,13,18,19,21,32–34,41,39]. Blaha and Langenecker [3], Langenecker [18,19] investigated the effect of superimposed high frequency ultrasonic energy during tension and compression tests of different metals. It was found that during the deformation, application of ultrasonic energy to the specimen reduces the yield strength of the material. This effect was similar to thermal softening, however, experimental results [3,18,19] revealed that the ultrasonic energy required to produce the same amount of softening is 10^7 times less than the required thermal energy. The reason is that ultrasonic energy is only absorbed in localized regions, such as vacancies, dislocations and grain boundaries, while thermal energy is absorbed uniformly in the material. Green [9], Mordyuk [23] and Severdenko et al. [29] performed experiments on different materials to study the effect of applying ultrasonic energy during deformation. Acoustic softening effects were observed and it was found that the reduction in yield strength is proportional to the applied ultrasonic intensity. Also, reduction in yield strength was found to be independent of ultrasonic frequency in the range of 15–18 kHz.

Researchers have started to work on developing methods to utilize acoustic softening during manufacturing. Langenecker [19] used ultrasonic energy during metal forming and showed that it could reduce the amount of force required to iron and deep-draw copper shells from 220 lb to 70 lb. Recent rapid manufacturing processes, for example ultrasonic consolidation [15–17,32–34], have shown that ultrasonic (acoustic) softening effects could help reduce the process time. Ashida and Aoyama [2] performed experimental and numerical studies of press forming by using superimposed ultrasonic energy supplied to the die. It was found that by using ultrasonic energy, wrinkling and cracking could be avoided. The results showed that this was achieved by reducing the friction force between the sheet metal and the die. For numerical purposes, the simulations were performed by manually selecting a higher friction coefficient for the case of press forming without ultrasonic energy and a lower friction coefficient for press forming with ultrasonic energy supplied to the die. Huang et al. [11] performed experimental studies on ultrasonic assisted upsetting processes and found that ultrasonic vibration reduced the average forming force during the upsetting due to the decrease in friction force. Hung and Hung [12] performed experimental studies on ultrasonic-vibration assisted hot upsetting of aluminum alloys. Temperature and strain rate effects during the ultrasonic assisted hot upsetting of aluminum were investigated. It was found that ultrasonic vibration reduces the compressive forces required during hot upsetting. Inoue [13] performed experimental studies on ultrasonic assisted metal tube drawing and found that, for thick steel tubes, no significant reduction in drawing force was observed. However, damages of the opening decreased and surface roughness and lifespan of the die were improved. Siddiq and Ghassemieh

* Corresponding author.
E-mail address: tamer.elsayed@kaust.edu.sa (T. El Sayed).

0041-624X/$ - see front matter © 2011 Elsevier B.V. All rights reserved.
doi:10.1016/j.ultras.2011.11.004

[32,34] reported that ultrasonic energy was not enough to cause acoustic softening in the material and only surface effects (friction) were dominant. Jimma et al. [14] performed experiments on ultrasonic assisted deep drawing processes and found that ultrasonic energy does not only reduce the drawing force but also increases the limiting drawing ratio. Li and Lang [20] also reported the reduction in drawing force due to ultrasonic energy and found that it also improved the lubrication condition between the wire and die. Lucas and Daud [21] performed simulations of ultrasonic assisted extrusion of aluminum using a conventional material model while varying the friction coefficient between the billet and the die to account for the effect of ultrasonic energy. However, it was reported that experimental results have shown acoustic softening in aluminum during ultrasonic assisted deformation, therefore, adjustments to the friction condition alone in the FE models are not sufficient to explain the measured reductions in extrusion force [4,21]. Murakawa et al. [24,25] performed experimental studies on ultrasonic assisted wire drawing by applying ultrasonic-vibration in both the radial and axial directions. They found that radial vibration is more effective in decreasing the drawing force and increasing the drawing speed as compared to axial vibration. Petukhow et al. [26] performed experimental studies on ultrasonic-assisted extrusion and found that ultrasonic energy reduces the friction force between the billet and die, eliminating the use of high viscosity lubricants. Rozner [27] performed experimental studies on ultrasonic assisted strip drawing and reported reduction in forming load. Susan and Bujoreanu [37] and Susan et al. [38] performed experimental and analytical studies on ultrasonic assisted wire drawing and also found that ultrasonic energy reduces the amount of forming force required. They also reported that ultrasonic energy reduces the work hardening level, which ultimately improves the ductility of the material during deformation.

In the aforementioned, most of the efforts in simulating the ultrasonic assisted manufacturing processes have concentrated on varying the friction coefficient to reduce the friction forces to account for the application of ultrasonic energy [2,5,10,21], i.e. reduction in the deforming forces and volume effects (acoustic softening) due to ultrasonic energy are not explicitly included in the utilized material models. Siddiq and Ghassemieh [32–34] incorporated the thermal and acoustic softening simultaneously in the conventional J2 plasticity framework. The motivation to incorporate acoustic softening in metals arises from the experimental studies in Blaha and Langenecker [3], Langenecker [18,19], Green [9], and Mordyuk [23] and theoretical studies in Rusynko [28] and Gilman [8]. It was reported that superimposed ultrasonic energy reduces the material's yield stress significantly. It was also reported that this is due to the contraction of the extended dislocations when traveling with a velocity higher than a critical speed. Due to the contraction of the extended dislocations, screw dislocations cross-glide freely without the aid of thermal activation. Therefore, the phenomenon is very different from thermal softening and requires ultrasonic energy of the order of magnitude 10^7 less than its thermal counterpart for the same amount of softening. This is due to the fact that thermal energy is absorbed uniformly in the specimen while ultrasonic energy is only absorbed in the regions of dislocations and defects. Therefore, processes which involve superimposed ultrasonic energy supplied to the specimen should be simulated using constitutive models that incorporate acoustic softening effects. Moreover, if relative motion of the surfaces (friction) exists then softening due to frictional heating should also be incorporated as surface effects [32]. Siddiq and Ghassemieh [32,35] found that in order to perform more realistic simulations of ultrasonic consolidation processes, both volume (acoustic softening) and surface (thermal softening due to friction) effects must be incorporated in the material model. It was found that during the ultrasonic consolidation process the material undergoes severe plastic deformation under compressive loading with superimposed ultrasonic energy [32–34,22,41]).

In general, during many of the ultrasonic assisted manufacturing processes, such as sheet metal press forming and wire drawing, the work piece is generally under tensile (uniaxial, biaxial or triaxial) loading. Conventional plasticity theory is based on constant volume assumption and works very well for materials with almost no microvoids [7]. However, in porous materials, volume does not remain constant due to the growth of microvoids during deformation. Therefore, due to the presence of these inherent microvoids in metals and alloys (depending upon the process of making such material), it is necessary to use a plasticity theory that takes into account the effect of porosity in the material during deformation. Weinberg et al. [40] proposed a variational constitutive model for porous materials with inherent microvoids. An energy function was derived based on the presence of spherical microvoids in the material. The volumetric plastic expansion was accounted for by incorporating the growth of voids and defects in metals during deformation. The theory was extended from small deformation to finite deformation by means of logarithmic and exponential mappings. It must be noted that the model takes into account the effect of the presence of microvoids during plastic deformation and can predict the damage initiation but not the damage evolution. For damage evolution during ductile failure, which is based on reaching the critical porosity during deformation and onsetting of the void coalescence, the reader is referred to the recent work by Siddiq et al. [36]. In the present work, a constitutive model that considers the effects of inherent porosity on the deformation behavior before and at damage initiation along with the effect of ultrasonic and frictional softening effects is used with the main focus on ultrasonic energy effects during the deformation. For this purpose, the variational elasto-visco-plastic theory for porous materials [40] is modified to incorporate the acoustic softening effects and utilized throughout this work. The conventional variational porous plasticity model [40] is summarized in the following. In this work, a fully variational porous plasticity constitutive model [40] is modified to account for acoustic softening effects and then utilized to simulate some of the ultrasonic assisted manufacturing processes. The versatility and predictive ability of the model is demonstrated by simulating three types of manufacturing processes: sheet metal press forming, wire drawing and hot upsetting. It must be noted that in the absence of the porosity, the model converges to the conventional J2 plasticity theory, already modified by Siddiq and Ghassemieh [32–34] to incorporate the thermal and acoustic softening effects.

The paper is organized as follows: In Section 2 we discuss the porous plasticity model of Weinberg et al. [40] and how it is modified to account for acoustic softening. In Section 3 we discuss the material parameters identification process and then we present the simulation results of various ultrasonic-assisted manufacturing processes and their validation against the experiments of Ashida and Aoyama [2], Daud et al. [4,5], Hung and Hung [12], and Murakawa et al. [24] in Section 4 followed by conclusions.

2. Variational porous plasticity with thermal and acoustic softening

2.1. Constitutive equations

A Helmholtz free-energy for the thermo-mechanical response is defined as a function of the deformation gradient F, the plastic part of the deformation gradient F^p, an effective deviatoric plastic strain ε^p, an effective volumetric plastic strain θ^p, and the absolute temperature T, and the ultrasonic intensity (rate of ultrasonic energy per unit area) E_u.

$$A = A(\boldsymbol{F}, \boldsymbol{F}^p, \varepsilon^p, \theta^p, T, E_u) \tag{2.1}$$

The plastic deformation rate is defined by

$$\dot{\boldsymbol{F}}^p \boldsymbol{F}^{p-1} = \dot{\theta}^p \boldsymbol{N}^p + \dot{\epsilon}^p \boldsymbol{M}^p \tag{2.2}$$

To ensure the irreversibility of plastic flow

$$\dot{\epsilon}^p \geqslant 0, \quad \dot{\theta}^p \geqslant 0 \tag{2.3}$$

The tensors $\boldsymbol{M}^p$ and $\boldsymbol{N}^p$ defines the direction of deviatoric and volumetric plastic strain rates, respectively, with the following conditions to be satisfied [40]

$$\mathrm{tr}(\boldsymbol{M}^p) = 0, \quad \boldsymbol{M}^p \cdot \boldsymbol{M}^p = \frac{3}{2}, \quad \boldsymbol{N}^p = \pm\frac{1}{3}\boldsymbol{I} \tag{2.4}$$

For purely volumetric deformations the flow rule (2.2) becomes

$$\frac{d}{dt}\log J^p = \mathrm{tr}(\boldsymbol{N}^p)\dot{\theta}^p = \pm\dot{\theta}^p \tag{2.5}$$

where the plus and minus signs in Eqs. (2.4) and (2.5) correspond to void expansion and collapse, respectively. The first Piola–Kirchhoff stress tensor is computed using

$$\boldsymbol{P} = \frac{\partial A}{\partial \boldsymbol{F}} \tag{2.6}$$

$\boldsymbol{T}^p$ and $\boldsymbol{Y}^p = \{Y^p, Z^p\}$ denote the thermodynamic forces conjugate to $\boldsymbol{F}^p$ and $\boldsymbol{Z}^p = \{\theta^p, \epsilon^p\}$, respectively, which are obtained by applying the chain rule, as follows:

$$\boldsymbol{T}^p = -\frac{\partial A}{\partial \boldsymbol{F}} \cdot \frac{\partial \boldsymbol{F}}{\partial \boldsymbol{F}^p} - \frac{\partial A}{\partial \boldsymbol{F}^p} = \boldsymbol{F}^{eT}\boldsymbol{P} - A_{,\boldsymbol{F}^p}, \tag{2.7}$$

$$Y^p = p - p_c, \quad Z^p = \sigma - \sigma_c, \tag{2.8}$$

where

$$p = -\frac{dA}{d\theta^p} = \boldsymbol{T}^p \cdot \boldsymbol{N}^p \boldsymbol{F}^p, \quad p_c = \frac{\partial A}{\partial \theta^p}, \tag{2.9}$$

$$\sigma = -\frac{dA}{d\epsilon^p} = \boldsymbol{T}^p \cdot \boldsymbol{M}^p \boldsymbol{F}^p, \quad \sigma_c = \frac{\partial A}{\partial \epsilon^p}, \tag{2.10}$$

and in which p and σ are the effective pressure and the effective deviatoric stress, respectively; and p_c and σ_c are the flow pressure and the deviatoric flow stress, respectively.

2.2. Void growth model

A void growth model is used based on the assumption that voids are spherical and remain spherical during deformation [40]. The local volume fraction of spherical voids in undeformed configuration is given by

$$f_0 = N_v \frac{4\pi a_0^3}{3} \tag{2.11}$$

where N_v is the void density, i.e. number of voids per unit volume and a_0 is the initial mean void radius. In order to find the evolution of the mean void radius (i.e. porosity) during the intermediate or plastically deformed configuration following relation was proposed (with the underlying assumptions of spherical shell model with a plastically incompressible matrix and elastic volume change of voids being negligible).

$$f = \frac{f_0 + J^p - 1}{J^p} \tag{2.12}$$

2.3. Strain energy density

The free energy density (2.1) is defined using an additive decomposition into elastic and plastic parts

$$A(\boldsymbol{F}, \boldsymbol{F}^p, \varepsilon^p, \theta^p, T, E_u) = W^e(\boldsymbol{F}\boldsymbol{F}^{p-1}, T) + W^p(\varepsilon^p, \theta^p, T, E_u) \tag{2.13}$$

where the superscripts e and p denote the elastic and plastic parts of the respective variables/functions.

The elastic strain energy density is defined as

$$W^e(\varepsilon^e, T) = W^{e,\mathrm{vol}}(\theta^e, T) + W^{e,\mathrm{dev}}(e^e, T) \tag{2.14}$$

$$W^{e,\mathrm{vol}}(\theta^e, T) = \frac{\kappa}{2}[\theta^e - \alpha(T - T_0)]^2 + \rho_0 C_v T\left(1 - \log\frac{T}{T_0}\right) \tag{2.15}$$

$$W^{e,\mathrm{dev}}(e^e, T) = \mu\|dev(\varepsilon^e)\|^2 \tag{2.16}$$

where $\theta^e = \log J^e$, κ is the bulk modulus, μ is the shear modulus, α is the thermal expansion coefficient, T_0 is a reference absolute temperature, and C_v is the specific heat per unit mass at constant volume. Similar to the elastic strain energy density, the plastic stored energy is also assumed to be the sum of volumetric and deviatoric components. The deviatoric part is defined as a conventional power-law hardening while the volumetric part is the sum of the plastic energy stored by each individual void. The relationships are given below

$$W^p(\varepsilon^p, \theta^p, T, E_u) = W^{p,\mathrm{vol}}(\theta^p, T, E_u) + W^{p,\mathrm{dev}}(\varepsilon^p, T, E_u) \tag{2.17}$$

$$W^{p,\mathrm{dev}}(\varepsilon^p, T, E_u) = \frac{n\sigma_0(T, E_u)\varepsilon_0^p}{n+1}\left(1 + \frac{\varepsilon^p}{\varepsilon_0^p}\right)^{\frac{n+1}{n}} \tag{2.18}$$

$$W^{p,\mathrm{vol}}(\theta^p, T, E_u) = \frac{n\sigma_0(T, E_u)\varepsilon_0^p}{n+1} N_v \frac{4\pi a^3}{3} g(\theta^p, n) \tag{2.19}$$

where

$$g(\theta^p, n) = \int_1^{1/f}\left(1 + \frac{2}{3\epsilon_0^p}\log\frac{x}{x - 1 + \frac{f_0}{f_0 + \exp\theta^p - 1}}\right)^{\frac{n+1}{n}} dx \tag{2.20}$$

where n is the hardening exponent, $\sigma_0(T)$ is the yield stress, and ε_0^p is the reference deviatoric plastic strain.

A phenomenological approach similar to the one presented in Siddiq and Ghassemieh [32–34] is used with the underlying assumptions for acoustic softening being based on experimental studies performed on different materials during ultrasonic assisted deformation [3,9,18,19,23,29]. These assumptions are: the reduction in yield strength is proportional to ultrasonic intensity and independent of frequency (in the range of 15–180 kHz), temperature (in the range of 30–500 °C) and residual stresses [32–34]. The suggested acoustic softening term is $(1 - d \cdot E_u)^e$. It must be noted that $e = 2$ was used for aluminum alloys in Siddiq and Ghassemieh [32–34] in the softening relationship. However, in the present study e has been set as an independent coefficient and the choice of e gives more flexibility during the parameter identification process. It must be noted that the parameters d and e cannot be identified using a single tensile (or compression) test; a number of tests performed using different levels of rate of ultrasonic energy per unit area supplied to the specimen would be required. Also, the acoustic softening parameters d and e will be different for different materials depending on the material's inherent microstructure, therefore generalization of these parameters is an interesting topic to be demonstrated in future works. It should be noted that ultrasonic intensity (E_u) is an observable variable and therefore the general framework of the conventional porous plasticity theory is kept preserved. The relation for yield stress with thermal and acoustic softening effects is given by

$$\sigma_0(T) = \sigma_0(T_0)\left(1 - \frac{T - T_0}{T_m}\right)^l (1 - d \cdot E_u)^e \tag{2.21}$$

where T_0 is the reference temperature, T_m is the melting temperature and l is the thermal-softening exponent. The rate sensitivity and micro-inertia parts of the theory are not discussed here, as were never activated during this work. Ultrasonic intensity E_u is the rate

of ultrasonic wave energy passing through an area and is defined as [30,31]

$$E_u = \frac{\sigma^2_{acoustic}}{\rho c} \tag{2.22}$$

with acoustic stress $\sigma_{acoustic} = \rho v c$, v being the velocity of a specific material point and c being the velocity of sound in the medium. The velocity of each material point at every increment of time is used to compute the acoustic stress and then rate of ultrasonic wave energy per unit area (2.22). For every wave cycle, updated values of rate of ultrasonic wave energy per unit area are averaged and then transferred to the modified porous plasticity constitutive model.

2.4. Variational constitutive updates

This section summarizes the incremental solution procedure used in the constitutive updates. Time is discretized as t_n(past) and t_{n+1} (present). Based on the past solution at time t_n, the state of the material $\left(F^p_n, \epsilon^p_n, \theta^p_n, \dot{\theta}^p_n, \theta^{\ddot{p}}_n\right)$ is assumed to be known. At time t_{n+1}, the constitutive model is called with the known deformation gradient F_{n+1}, temperature T_{n+1} and ultrasonic intensity $E_{u,n+1}$. This means that the unknown state variables of the material at time t_{n+1} are F^p_{n+1}, ϵ^p_{n+1}, θ^p_{n+1}, $\dot{\theta}^p_{n+1}$, $\theta^{\ddot{p}}_{n+1}$ along with the directions M, N of the incremental plastic deformation. The update is expressed in a variational form, similar to Weinberg et al. [40] as

$$W_n(F_{n+1}, T_{n+1}, E_{u,n+1}) = \min_{\epsilon^p_{n+1}, \theta^p_{n+1}, M, N} f_n\left(F_{n+1}, T_{n+1}, E_{u,n+1}, \epsilon^p_{n+1}, \theta^p_{n+1}, M, N\right)$$

which is subjected to the constraint Eqs. (2.3) and (2.4).

The minimization of the above variational form returns the updated values of the unknown state variables and plastic flow directions. It must be noted that the minimization of the above is the effective incremental strain-energy density which acts as a potential for the first Piola–Kirchhoff stress tensor P_{n+1} at time t_{n+1} (2.6). The tangent moduli DP_{n+1} is obtained by the linearization of Eq. (2.6). A predictor–corrector strategy based on logarithmic elastic strains is used to solve the incremental variational problem. This strategy reduces the finite deformation constitutive updates to small strains and purely kinematic steps (for details see Weinberg et al. [40] and references therein).

The modifications were incorporated into the ABAQUS user material subroutine for explicit analysis (VUMAT). The material parameter identification procedure using experimental test data is presented in the following section.

3. Material parameters identification

To demonstrate the performance of the modified theory, a uniaxial tension test of soft aluminum grade with and without ultrasonic energy is simulated and validated against the experimental results [5]. Experimental and simulation test conditions were the same, i.e. a constant crosshead speed of 5 mm/min with and without ultrasonic energy. The ultrasonic energy was supplied with a frequency of 20 kHz and an amplitude of vibration equals to 10 μm. Fig. 3.1 shows the calibration of the constitutive model parameters using the experimental uniaxial tension test data in Daud et al. [5]. There was no ultrasonic energy supplied to the system during the experiments or in the simulations. Model predictions show a good agreement with experimental results. The identified set of parameters is given in Table 1. The parameters identified via quasi-static tests include the initial yield strength (σ_0), the reference deviatoric plastic strain (ε^p_0), hardening exponent (n), void radius (a_0) and void density (N). Predetermined thermal properties used throughout this work are taken from Siddiq and Ghassemieh [32].

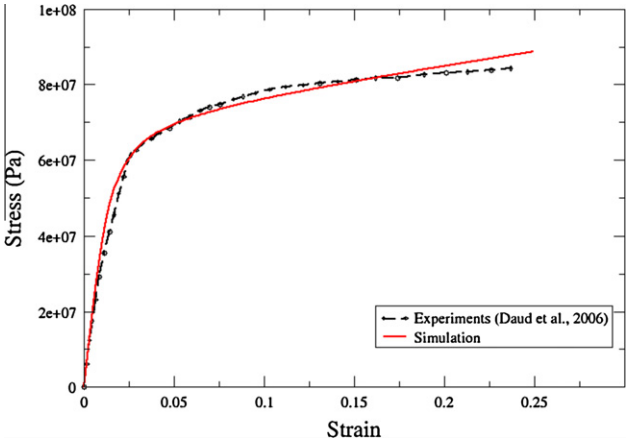

Fig. 3.1. Comparison of experimental data with presented constitutive model without ultrasonic energy.

For the identification of the ultrasonic softening parameters, a second set of experimental stress–strain data is used with the previously identified deformation parameters. For this case, ultrasonic energy is applied to the system for two different intervals of time, as was in the experiments [5]. During the first interval, ultrasonic energy is applied for an approximate duration of 6 s and then discontinued for 6 s. During this time, the specimen was allowed to deform. The second phase of ultrasonic energy was applied for 12 s and then discontinued [5]. Similar conditions were used during the simulations to identify the ultrasonic softening parameters. Comparison of the experimental results [5] and simulation results is shown in Fig. 3.2. The identified set of parameters is given in Table 1. The results show good agreement between the experimental and simulated response. In order to demonstrate the applicability of the proposed model, three different ultrasonic assisted manufacturing processes are simulated and discussed in the following sections.

4. Application to ultrasonic assisted manufacturing processes

Three different ultrasonic assisted manufacturing processes are simulated using the presented porous plasticity model. All the performed computations were fully coupled thermal and stress analyses in ABAQUS/Explicit [1]. The results of the simulations are discussed in what follows.

4.1. Ultrasonic assisted sheet metal forming

Sheet metal forming has been used in manufacturing different components in the industry for many decades. In general, the primary setup involves a die and a punch that converts a sheet of material into the desired shape. In order to reduce friction between the die and the work piece, lubricants are used. However, use of lubricants is generally restricted due to environmental concerns. Therefore, researchers have been working on developing techniques to reduce the friction forces between the die and the material sheet to avoid failure. Ultrasonic assisted sheet metal forming processes provide the possibility of reducing the friction forces [2,11–15,25,24,27,37,38]. In this section, ultrasonic assisted sheet metal forming similar to Ashida and Aoyama [2] is simulated using the presented porous plasticity model with acoustic softening. Experimental studies [2] were performed on sheet metal forming with and without ultrasonic vibration. It was found that the

Table 1
Material parameters for aluminum grade 1050.

E (GPa)	v	ρ_0 (kg m^{-3})	T_0 (K)	T_m (K)	l	α (K^{-1})	k (W/m K)	C_v (J/kg K)
Predetermined parameters								
2.50	0.33	3600	293	933	0.75	23.4e-6	235	896
σ_0 (T_0)	ε_0^p	n	a_0 (μm)	N (m^{-3})				
Parameters determined by quasi-static tensile tests								
53	0.01	14.605	100	10^8				
d (m^2/W)	e							
Parameters determined by the discontinuous ultrasonic assisted tensile test								
2.3e−7	2.0							

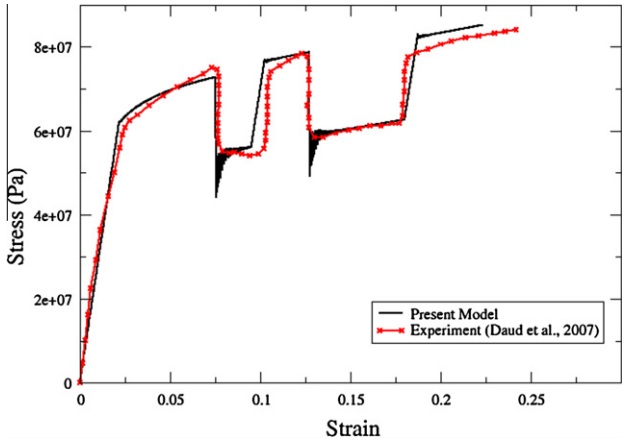

Fig. 3.2. Uniaxial tension test with ultrasonic energy applied for small intervals of time.

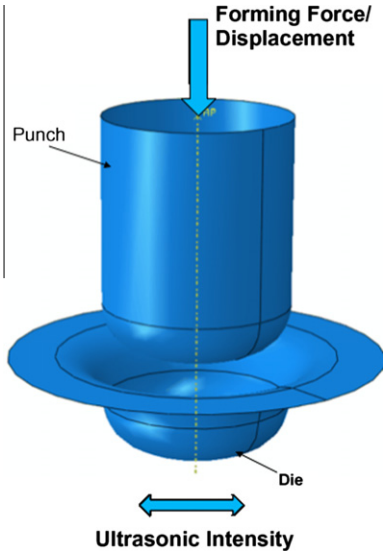

Fig. 4.1. Schematic of the sheet metal forming model.

friction force is reduced when ultrasonic energy (frequency = 19.5 kHz; amplitude = 11.4 μm) is supplied to the die. Also, the material was successfully formed without failure. It was also reported that due to high friction, the material fractured when forming was done without ultrasonic energy. The results were then simulated using a specialized press-forming tool, with and without ultrasonic energy by manually varying the friction coefficient. A higher value for the coefficient of friction was used when no ultrasonic energy is applied to the die and a lower value when ultrasonic energy is applied.

Sheet metal forming simulations similar to Ashida and Aoyama [2] are performed in this section. An approximate geometry of the die and punch is modeled (see Fig. 4.1) and the results are compared in a qualitative manner. The aim of these simulations is to explore the observation of reduction in friction forces when ultrasonic energy is supplied to the die and to show the applicability of the proposed material model in the simulation of ultrasonic assisted forming processes.

The materials parameters used for the metal sheet are listed in Table 1. The punch speed used in all the simulations is 6.7 mm/s and is applied from the top of the punch as shown in Fig. 4.1 while ultrasonic oscillations are supplied simultaneously in the direction orthogonal to the vertical direction (punch loading direction). This is achieved by fixing the die in the vertical direction and only allowing it to move in the direction of ultrasonic oscillation as shown in Fig. 4.1. In order to apply ultrasonic oscillation, displacement boundary conditions with a periodic amplitude curve ($A = A_{max} \sin \omega t$) are used, where A is the amplitude of the vibration dependent on time, A_{max} is the maximum amplitude of the vibration, ω is the angular velocity related to the frequency of vibration and t is the total time. Three different cases have been simulated with different levels of ultrasonic energy supplied to the die:

- No ultrasonic energy (conventional forming)
- Ultrasonic energy with frequency = 19.5 kHz and amplitude = 2.5 μm
- Ultrasonic energy with frequency = 19.5 kHz and amplitude = 11.5 μm

Contour plots of the friction force between the die and the blank at different deformation stages are shown in Fig. 4.2. Friction forces reported in this section are the magnitude of the components of the nodal friction force vector in the contact domain. It should be noted that the coefficient of friction was kept constant throughout the simulations and friction force was allowed to vary with the contact pressure. It can be inferred from Fig. 4.2 that as the deformation increases, the friction force also increases due to the higher contact pressure between the die and the blank. A comparison of the friction forces at the end of the forming process is shown in Fig. 4.3. It is also shown that ultrasonic energy plays a role in reducing the friction force due to acoustic softening. Moreover, as the amplitude of ultrasonic vibration is increased, the distribution of the friction force becomes more uniform due to material softening. The present porous plasticity model with acoustic softening effects captures this phenomenon as observed during the experiments.

Forming forces applied through the punch are plotted as a function of the forming process simulation time in Fig. 4.4. It can be inferred that as the deformation goes on, the forming force increases. Also, as the ultrasonic intensity increases (by virtue of increase in amplitude of ultrasonic vibration), the amount of forming force

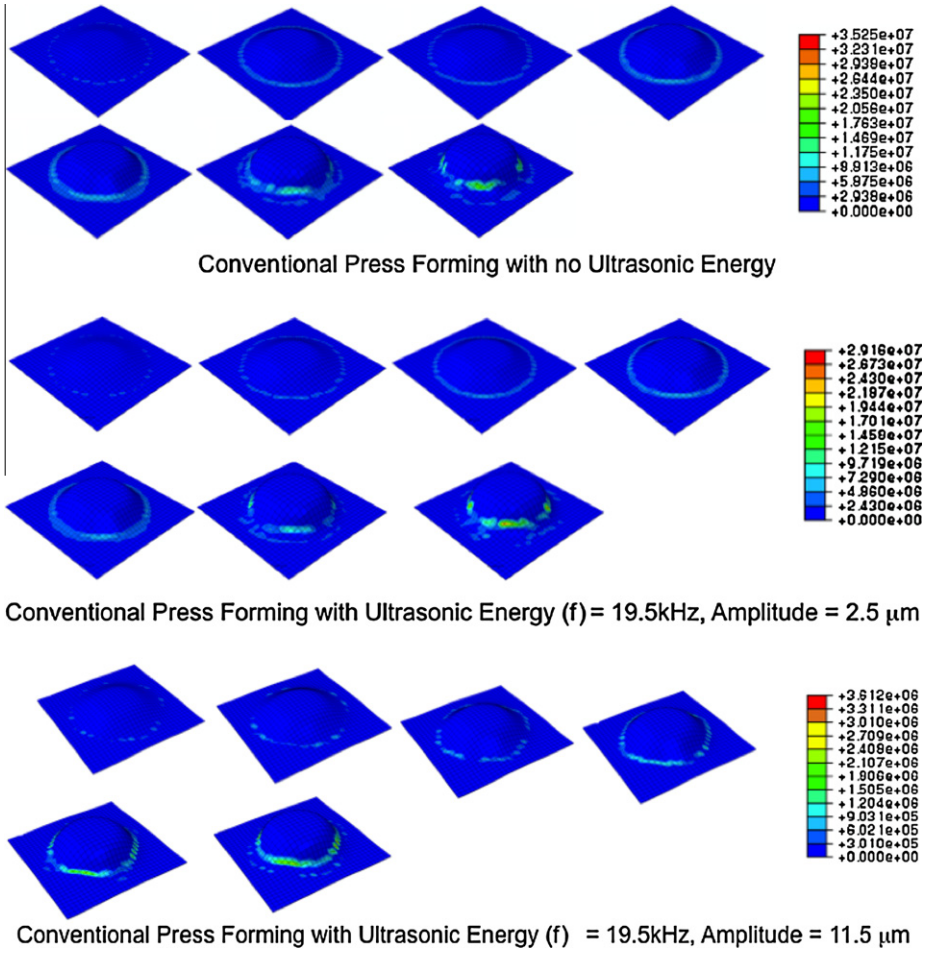

Fig. 4.2. Contour plots of friction force (10^{-3} N) between die and blank 0, 2.5 and 11.5 μm (from top to bottom).

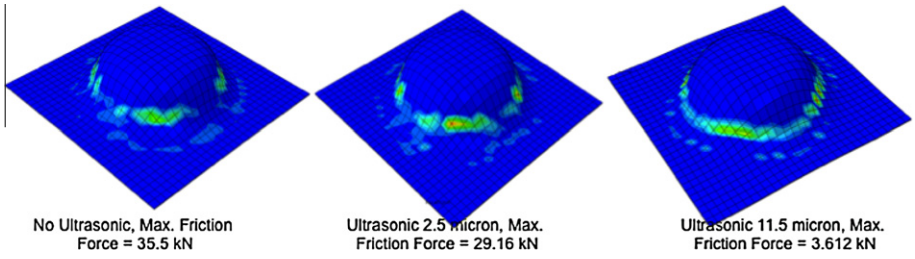

Fig. 4.3. Contour plots of the friction force at the end of the deformation for the three cases.

required decreases. As explained before, this is due to the thermal and acoustic softening effects in the vicinity of the contact regions of the die and the metal sheet. As suggested by Langenecker [19], this opens a new venue to increase the punch speed during sheet metal forming resulting in higher production rates. Also, a press machine with a lower load capacity can be used to form tough materials that usually require higher loads during conventional pressing by the application of ultrasonic energy to the dies.

In order to demonstrate the significance of using porous plasticity theory, simulations for the case when ultrasonic energy is applied with a frequency of 19.5 kHz and amplitude of 11.5 μm are performed varying the initial porosity of the material. The required forming force during the ultrasonic assisted process is plotted for the total duration of the process in Fig. 4.5. Interestingly, it is found that the forming force starts to decrease at the end of the forming process due to the void growth causing additional material softening than ultrasonic softening, however, the difference is small at this stage as shown in an exaggerated view of the force time curve on the right side of Fig. 4.5.

In order to further investigate this issue, evolution of porosity is plotted as a function of the process time in Fig. 4.6. Evolution of porosity has been recorded in the region that showed maximum volumetric plastic strain as shown in Fig. 4.7. As expected, it is found that the porosity remains constant (equals to the initial porosity) until a point where it starts to increase. It can be inferred from Fig. 4.6 that in the present case the evolution of porosity (void growth) starts at the end of the simulation and this is why the forming forces start to decrease after certain amount of deformation (as shown in Fig. 4.5). Fig. 4.6 also explains that as the initial porosity is increased, the slope of the evolution curve decreases causing the forming force with lower initial porosity to show higher degradation than the one with higher initial porosity. Fig. 4.7

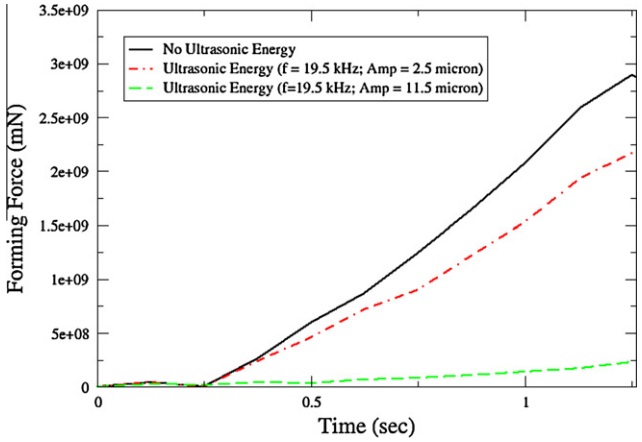

Fig. 4.4. Forming force as a function of time for three different levels of ultrasonic intensity.

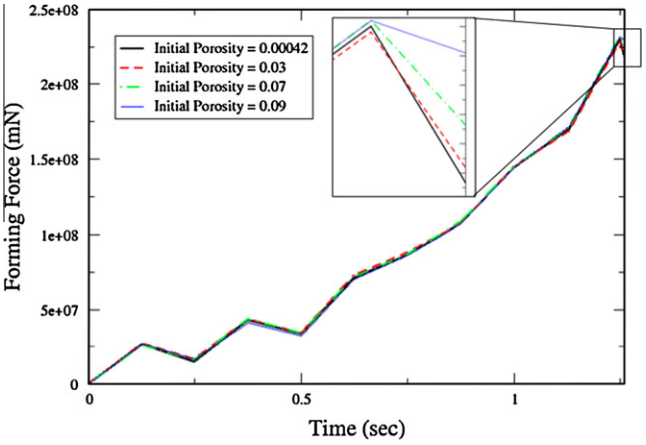

Fig. 4.5. Effect of initial porosity in the metal on the forming force.

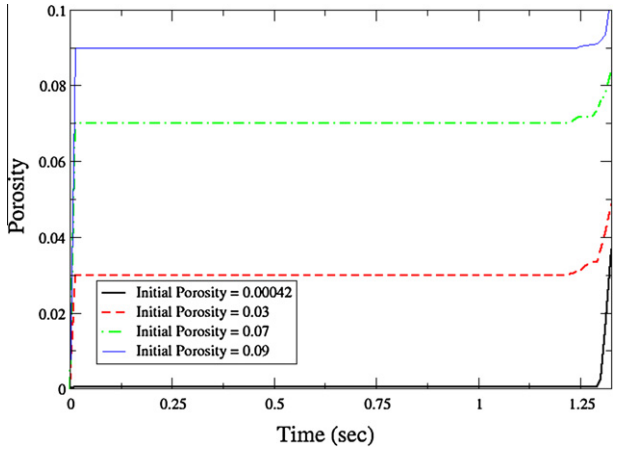

Fig. 4.6. Evolution of porosity during the forming process.

shows the regions with maximum volumetric plastic strain that corresponds to the maximum evolution of porosity. These are the regions which are more prone to failure if further deformed due to void growth followed by void coalescence. Similar failure modes have been reported by Djavanroodi and Derogar [6] for a similar type of sheet metal forming die. As discussed previously, the model only incorporates the material softening due to void growth until it reaches to a critical porosity (critical volumetric plastic strain), i.e.

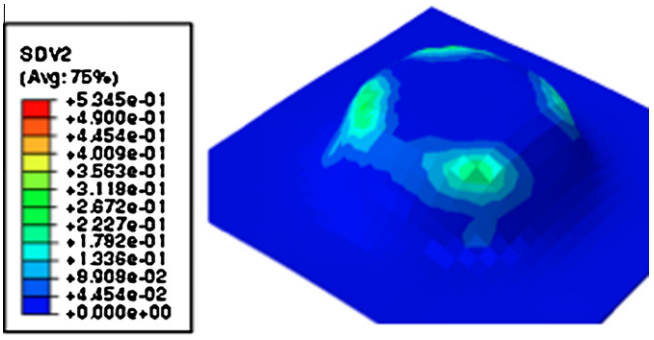

Fig. 4.7. Region of maximum porosity at the end of forming process.

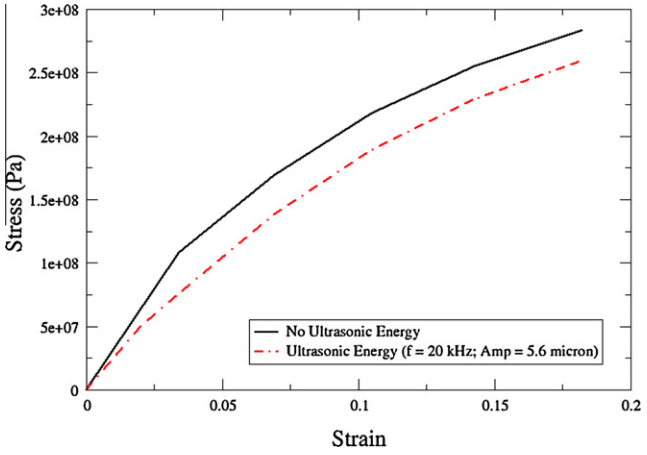

Fig. 4.8. Effect of ultrasonic energy on the stress strain behavior during upsetting of aluminum.

damage initiation, for damage evolution part, a recently published void coalescence model by the authors [36] should be used.

4.2. Ultrasonic assisted upsetting

To further demonstrate the predictive ability of the presented model, ultrasonic assisted upsetting of aluminum alloy [12] is simulated at room temperature. The simulation conditions used were the same as in the experiments. The specimen size was 6 mm high and 6 mm diameter. The frequency of ultrasonic vibration was 20 kHz and the amplitude was 5.6 μm. The strain rate during the deformation was 0.03/s. The material parameters used are summarized in Table 1. The selection of these parameters is based on the fact that the properties of the aluminum alloy used in Hung and Hung [12] are almost the same as for the aluminum used in the parameter identification process. Simulations were performed for the cases of no ultrasonic energy supplied and ultrasonic energy supplied with frequency and amplitude as described above. Fig. 4.8 shows the stress–strain response for the two cases. It is found that ultrasonic energy reduces the stress strain response of the material during the upsetting process due to acoustic softening. An explicit comparison between the experimental stress–strain response and the simulations is shown in Fig. 4.9. The results show a very good agreement between the experimental and simulated response.

4.3. Ultrasonic assisted wire drawing

Ultrasonic wire drawing processes have been in use for the past decade [10,14,20,24,37,38]. As discussed before, most of them have

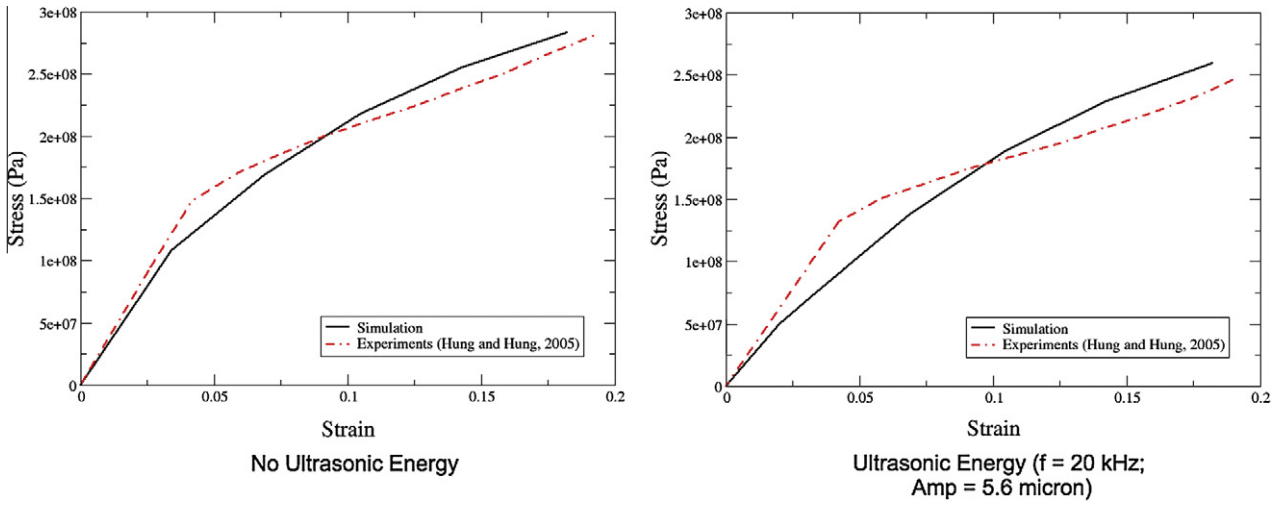

Fig. 4.9. Comparison of stress–strain response for upsetting of aluminum with and without superimposed ultrasonic energy.

reported a decrease in the drawing force when ultrasonic energy is applied to the system. In this work, using the same set of parameters in Table 1, an ultrasonic assisted drawing process is simulated. The simulation conditions are kept the same as were in the experimental ultrasonic drawing of Murakawa and Jin [24]. The specimen size was 6.0 mm in diameter and the reduction ratio was 6.6%. The ultrasonic energy is supplied with a frequency of 15 kHz and simulations are performed for four different levels of ultrasonic energies:

- No ultrasonic energy (conventional drawing).
- Ultrasonic energy with amplitude of 1 μm.
- Ultrasonic energy with amplitude of 2.5 μm.
- Ultrasonic energy with amplitude of 10 μm.

Drawing stress as a function of drawing speed is plotted in Fig. 4.10. Drawing stress is computed using the drawing force at the pulling end over the cross-sectional area of the pulling end of the wire. It is found that as the drawing speed increases, the drawing stress (force) also increases. However, the increase in the drawing stress is small. For the case when an ultrasonic energy with amplitude of 1 μm is applied to the system there is no effect of ultrasonic intensity on the drawing stress until the drawing speed used is smaller than ~300 mm/s. Below this velocity, the drawing stress starts to decrease at a faster rate than the conventional drawing stress. This is due to the decrease in the drawing

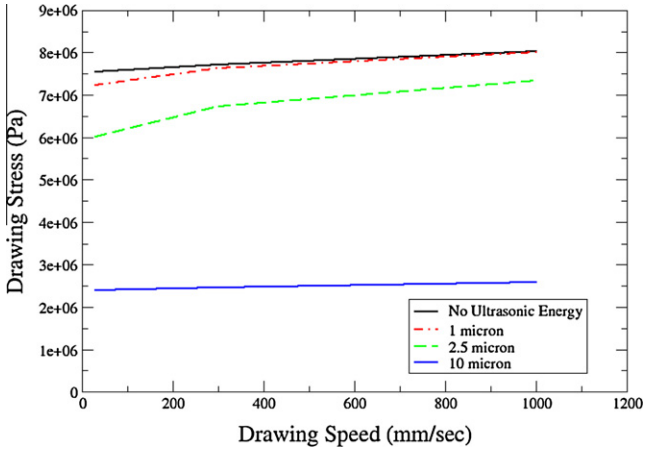

Fig. 4.10. Effect of ultrasonic energy and drawing speed on drawing stress.

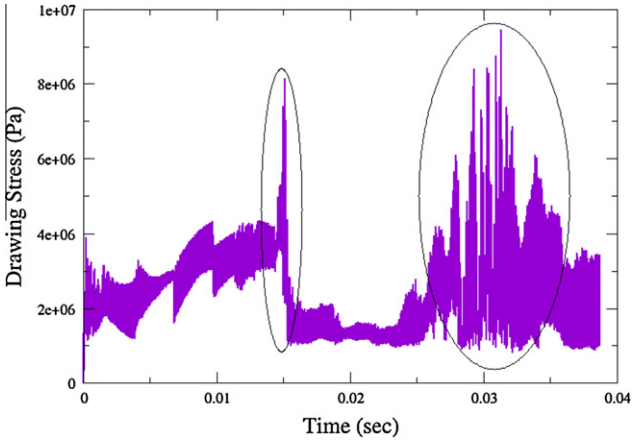

Fig. 4.11. High fluctuations in drawing stress for the case when amplitude was 10 μm and drawing speed was 300 mm/s.

speed, which gives more time for the material to soften in the die due to the ultrasonic energy. For different levels of ultrasonic energy supplied to the system, i.e. 1 μm, 2.5 μm and 10 μm, there is increase in acoustic softening as the amplitude of ultrasonic vibration is increased due to the increase in intensity of the supplied energy. It can also be inferred from Fig. 4.10 that the slope of the drawing stress versus drawing speed decreases as the amplitude of the ultrasonic vibration increases. This means that in order to reach the same amount of drawing stress, one can use a very high drawing speed. This is the reason why ultrasonic assisted wire drawing falls into the category of rapid manufacturing processes, i.e. by applying ultrasonic energy one can reduce the production time. However, it must be noted that during the simulation for the case when ultrasonic vibration amplitude of 10 μm is used, there were intense jerks observed in the drawing stress–time curve (Fig. 4.11). This shows the limitation that the ultrasonic amplitude must not exceed a certain limit, beyond which the separation between the die and wire surface will cause scratches in the specimen [24].

5. Conclusions

A fully variational porous metal plasticity model has been modified to incorporate acoustic softening experienced by porous

metals undergoing ultrasonic assisted deformation processes. The effect of acoustic softening is included in the constitutive model while keeping the general framework of the constitutive updates preserved. Results of three different ultrasonic assisted manufacturing processes have been presented and the critical role ultrasonic energy plays in reducing the friction and forming forces during deformation is demonstrated. Moreover, the evolution of porosity during sheet metal forming and its effect on the forming force have been investigated. Future work may include the incorporation of void coalescence in the presented porous plasticity model. This will enable the modeling of ductile failure during forming, which is primarily caused by void coalescence.

Acknowledgment

This work was fully funded by KAUST's baseline fund.

References

[1] ABAQUS, ABAQUS 6.9 Documentation, DS SIMULIA, 2009.
[2] Y. Ashida, H. Aoyama, Press forming using ultrasonic vibration, Journal of Materials Processing Technology 187–188 (2007) 118–122.
[3] F. Blaha, B. Langenecker, Tensile deformation of zinc crystal under ultrasonic vibration, Naturwissenschaften 42 (1955) 556.
[4] Y. Daud, M. Lucas, Z. Huang, Ultrasonic compression tests on aluminium, Applied Mechanics and Materials 3–4 (2005) 99–104.
[5] Y. Daud, M. Lucas, Z. Huang, Modelling the effects of superimposed ultrasonic vibrations on tension and compression tests of aluminium, Journal of Materials Processing Technology 186 (2007) 179–190.
[6] F. Djavanroodi, A. Derogar, Experimental and numerical evaluation of forming limit diagram for Ti6Al4V titanium and Al6061-T6 aluminium alloys sheets, Materials and Design (2010), doi:10.1016/J.matdes.2010.05.030.
[7] M.S. Gadala, M.L. Mullins, M.A. Dokainish, A modified plasticity theory for porous metals, International Journal for Numerical Methods in Engineering 15 (1980) 649–660.
[8] J.J. Gilman, Contraction of extended dislocations at high speeds, Materials Science and Engineering A 319–321 (2001) 84–86.
[9] R.E. Green, Non-linear effects of high-power ultrasonics in crystalline solids, Ultrasonics 13 (1975) 117–127.
[10] M. Hayashi, M. Jin, S. Thipprakmas, M. Murakawa, J. Hung, C. Tsai, Y. Hung, Simulation of ultrasonic-vibration drawing using the finite element method (FEM), Journal of Materials Processing Technology 140 (2003) 30–35.
[11] Z. Huang, M. Lucas, M.J. Adams, Influence of ultrasonics on upsetting of a model paste, Ultrasonics 40 (2002) 43–48.
[12] J. Hung, C. Hung, The influence of ultrasonic-vibration on hot upsetting of aluminium alloy, Ultrasonics 43 (2005) 692–698.
[13] M. Inoue, Studies on ultrasonic metal tube drawing, Memoira of Sagami Institute of Technology 19 (1984) 1–7.
[14] T. Jimma, Y. Kasuga, N. Iwaki, O. Miyazawa, E. Mori, K. Katsuhiko, H. Hatano, An application of ultrasonic vibration to the deep drawing process, Journal of Materials Processing Technology 80–81 (1998) 406–412.
[15] C.Y. Kong, R.C. Soar, P.M. Dickens, Characterization of aluminium alloy 6061 for the ultrasonic consolidation process, Materials Science and Engineering A 360 (2003) 99–106.
[16] C.Y. Kong, R.C. Soar, P.M. Dickens, A model for weld strength in ultrasonically consolidated components, in: Proc. IMechE Part C: J. Mech. Eng. Sci, 2004, pp. 83–91.
[17] C.Y. Kong, R.C. Soar, P.M. Dickens, Optimum process parameters for ultrasonic consolidation of aluminium alloy 3003, Journal of Materials Processing Technology 146 (2004) 181–187.
[18] B. Langenecker, Work-softening of metal crystals by alternating the rate of glide strain, Acta Metallurgica 9 (1961) 937–940.
[19] B. Langenecker, Effects of ultrasound on deformation characteristics of metals, IEEE Transactions on Sonics and Ultrasonics SU-13 (1966) 1–8.
[20] L. Li, X. Lang, Wire drawing with ultrasonic vibration, Journal Wire Industry 61 (1994) 721.
[21] M. Lucas, Y. Daud, A finite element model of ultrasonic extrusion, 7th International Conference on Modern Practice in Stress and Vibration Analysis, vol. 181, IOP Publishing Ltd., 2009. 012027-1.
[22] E. Mariani, E. Ghassemieh, Microstructure evolution of 6061 O Al alloy during ultrasonic consolidation: an insight from electron backscatter diffraction, Acta Materialia 58 (2010) 2492–2503.
[23] N.S. Mordyuk, Influence of Ultrasonic Oscillations on the Physical Properties of Metals and Alloys, Naukova Dumka, Kiev., 1975 (in Russian).
[24] M. Murakawa, M. Jin, The utility of radially and ultrasonically vibrated dies in the wire drawing process, Journal of Materials Processing Technology 113 (2001) 81–86.
[25] M. Murakawa, M. Jin, P. Kaewtatip, Utility of ultrasonic vibration applied to metal-forming processes, Advanced Technology of Plasticity (1999) 19–24.
[26] V.I. Petukhow, O.V. Abramov, A.M. Zubko, Y.V. Manegin, Extrusion of aluminium in an ultrasonic field, Light Metal Age 31 (1973) 6–8.
[27] A.G. Rozner, Effect of ultrasonic vibration on coefficient of friction during strip drawing, Journal of Acoustic Society of America 49 (1971) 1368–1371.
[28] A.K. Rusynko, Mathematical description of ultrasonic softening of metals within the framework of the synthetic theory of plasticity, Materials Science 37 (2001) 671–676.
[29] V.P. Severdenko, V.V. Klubovich, A.V. Stepanenko, Metal working under pressure with ultrasound, Nauka i Tkhnika, Minsk., 1973 (in Russian).
[30] A. Siddiq, T. El Sayed, Acoustic softening in metals during ultrasonic assisted deformation via CP-FEM, Materials Letters 65 (2011) 356–359.
[31] A. Siddiq, T. El Sayed, A thermomechanical crystal plasticity constitutive model for ultrasonic consolidation, Computational Materials Science 51 (2012) 241–251.
[32] A. Siddiq, E. Ghassemieh, Thermomechanical analyses of ultrasonic welding process using thermal and acoustic softening effects, Mechanics of Materials 40 (2008) 982–1000.
[33] A. Siddiq, E. Ghassemieh, Modelling and Characterization of Ultrasonic Consolidation Process on Aluminum Alloys, vol. 1079, pp. 125–132, San Fransisco, California, USA, 2008b, MRS Spring Meeting 2008.
[34] A. Siddiq, E. Ghassemieh, Theoretical and finite element analysis of ultrasonic welding of aluminum alloy 3003, Journal of Manufacturing Science and Engineering 131 (2009). 041007–1.
[35] A. Siddiq, E. Ghassemieh, Fibre embedding in aluminium alloy 3003 using ultrasonic consolidation process – thermomechanical analyses, International Journal of Advanced Manufacturing Technology 54 (2011) 997–1010.
[36] A. Siddiq, R. Arciniega, T. El Sayed, A variational void coalescence model for ductile metals, Computational Mechanics (2011), doi:10.1007/s00466-011-0639-9.
[37] M. Susan, L.G. Bujoreanu, The metal-tool contact friction at the ultrasonic vibration drawing of ball-bearing steel wires, Revesita de Metalurgia 35 (1999) 379–383.
[38] M. Susan, L.G. Bujoreanu, D.G. Galusca, C. Munteanu, M. Mantu, On the drawing in ultrasonic field of metallic wires with high mechanical resistance, Journal of Optoelectronics and Advanced Materials 7 (2005) 637–645.
[39] N.A. Tyapunina, V.V. Blagoveshchenskii, G.M. Zinenkova, Y.A. Ivashkin, Characteristics of plastic deformations under the action of ultrasound, Russian Physics Journal 25 (1983) 569–578.
[40] K. Weinberg, A. Mota, M. Ortiz, A variational constitutive model for porous metal plasticity, Computational Mechanics 37 (2006) 142–152.
[41] Z. Zhu, B.P. Wynne, E. Ghassemieh, A. Siddiq, Microstructural analysis of ultrasonic welded AA6061 by electron backscattered diffraction, Rare Metal Materials and Engineering 38 (2009) 147–151.